Optimization of quasi-solid-state dye-sensitized photovoltaic fibers using porous polymer electrolyte membranes

Jae Hong Kim [a], Yong Seung Chi [b], Tae Jin Kang [a],*

[a] Department of Materials Science and Engineering, Seoul National University, 599 Gwanak-ro, Gwanak-gu, Seoul 151-742, Republic of Korea
[b] Fashion Textile Center (FTC), Seoul National University, 599 Gwanak-ro, Gwanak-gu, Seoul 151-742, Republic of Korea

HIGHLIGHTS

► Dye-sensitized photovoltaic fibers were fabricated using electrolyte membranes.
► Membranes with different pore structure were obtained by varying the P123 content.
► The ionic conductivity of electrolyte membrane increased with higher P123 content.
► Enhanced conductivity resulted in superior performances of the photovoltaic fiber.
► The possibility for large-scale application of the photovoltaic fiber was confirmed.

ARTICLE INFO

ABSTRACT

Quasi-solid-state dye-sensitized photovoltaic fibers are fabricated using poly(vinylidenefluoride-co-hexafluoropropylene) (PVdF-HFP)/polyethylene oxide-co-polypropylene oxide-co-polyethylene oxide (P123) porous polymer electrolyte membranes and their photocurrent–voltage (I–V) characteristics are presented. The working electrode is a titanium wire coated with a dye-adsorbed TiO_2 layer and the counter electrode is a platinum wire coated with a porous polymer electrolyte membrane. Different pore structures in the PVdF-HFP/P123 polymer membranes are obtained by varying the blend ratio of the polymers. The overall pore volume increases with higher P123 content, improving the ionic conductivity of the porous polymer electrolyte membrane by facilitating the uptake of electrolyte solution. Consequently, quasi-solid-state dye-sensitized photovoltaic fibers fabricated with membranes higher in P123 content give superior performances. The photoelectrochemical characteristics of the photovoltaic fiber are also dependent upon the thickness of the TiO_2 layer and the twist pitch length of the counter electrode. The best performing photovoltaic fiber in this study exhibits a short-circuit current density (J_{sc}) of 2.117 mA cm^{-2}, open-circuit voltage (V_{oc}) of 0.6932 V, fill factor (FF) of 0.7015 and an energy conversion efficiency (η) of 1.029%. Finally, the possibility for large-scale application of the quasi-solid-state dye-sensitized photovoltaic fiber is confirmed by implementing a mesh-type weave structure based on fiber-like electrodes.

1. Introduction

Owing to its outstanding cost-effectiveness, simple fabrication process and fairly high conversion efficiency, dye-sensitized solar cells (DSSCs) have been under extensive research for over 20 years [1–4]. In general, DSSCs consist of a transparent conducting oxide (TCO) coated glass substrate, photosensitive dye-adsorbed oxide semiconductor nanoparticles, electrolytes and a counter electrode. The high rigidity of the TCO coated glass substrate used in DSSCs, however, limit the design, manufacturing process and application of the device [5–7]. Thus, flexible DSSCs using polymer substrates such as polyethylene terephthalate (PET) [8–12] and polyethylene naphthalate (PEN) [13–15] have been actively studied, but the low thermal resistance of such polymer substrates and their limited planar shape became new obstacles to overcome. Recently, dye-sensitized photovoltaic fibers using metal wire substrates have attracted interest as an approach to satisfy the requirements mentioned above, i.e. versatile design options, thermal stability against high-temperature sintering processes and flexibility.

A fiber based DSSC having a helical twisted structure was developed by Fan et al. [16] using TiO₂ coated stainless steel fibers and conducting fibers coated with protective layers. Ramier et al.

* Corresponding author. Tel.: +82 2 880 7197; fax: +82 2 885 9671.
E-mail address: taekang@snu.ac.kr (T.J. Kang).

[17,18] produced a wire based DSSC using TiO_2 layer coated titanium wires and confirmed its possible application in photovoltaic textiles by testing its mechanical characteristics. Wang et al. [19] took a different approach and fabricated a three-dimensional DSSC by directly growing TiO_2 nanowires on a spiral-shaped titanium wire and obtained a conversion efficiency of 0.86%. But, due to the usage of conventional liquid-state electrolytes, commercialization problems remain with wire-based DSSCs, such as poor long-term stability caused by leakage and volatilization of the electrolyte and the requirement of additional sealing processes. To solve the fundamental problems of liquid-state electrolytes and to take a step closer to commercialization of large-scale DSSC modules, several attempts applying solid-state electrolytes such as inorganic/organic p-type semiconductors [20–22], ionic liquid electrolytes [23–25] and polymer electrolytes [26–30] were recently reported. But most of these studies have been limited to planar DSSCs.

Toivola et al. [31] characterized photovoltaic fibers composed of gelatinized iodine electrolyte, a TiO_2 layer deposited optical fiber and a carbon based counter electrode. Fan et al. [32] fabricated fibrous solid-type DSSCs using a stainless steel wire and a copper wire as fiber-like electrodes and copper iodide as a solid-state electrolyte. The same group [33] also reported the improvement of conversion efficiency from 0.06% to 1.38% through surface engineering of a titanium wire and modification of the TiO_2 layer. Yu et al. [34] developed semi-solid and all-solid fiber-type DSSCs based on a cylindrical core-shell-like TiO_2 nanotube array photoelectrode and achieved a conversion efficiency of 1.5% for semi-solid and 0.21% for all-solid fiber-type DSSC. There is still much room for improvement in the application of solid-state electrolytes for dye-sensitized photovoltaic fibers.

Poly(vinylidenefluoride-co-hexafluoropropylene) (PVdF-HFP) copolymer, which consists of VdF and HFP units, is widely used as a polymer matrix for polymer electrolytes in lithium (Li) ion batteries [35–37]. In PVdF-HFP membranes, the crystalline VdF units provide excellent mechanical properties and chemical stability, whereas the amorphous HFP units contribute to the improvement of ionic conductivity by trapping large amounts of liquid-state electrolyte [36,37]. Thus, when immersed in a liquid electrolyte solution for some time, PVdF-HFP polymer electrolyte membranes show high conductivity of the order of 10^{-3} S cm^{-1}.

Our group [38] has recently applied porous polymer films in fiber-type DSSCs and reported that the pore structure in polymer films facilitated the penetration of electrolyte solution through the membrane and increased the contact area at the interface between the electrode and electrolyte, which eventually enhanced the photovoltaic performances of the fiber-type DSSCs. In this paper, quasi-solid-state dye-sensitized photovoltaic fibers using PVdF-HFP/P123 porous polymer electrolyte membranes are fabricated and their photovoltaic performances are investigated. The PVdF-HFP/P123 porous polymer electrolyte membranes are expected to
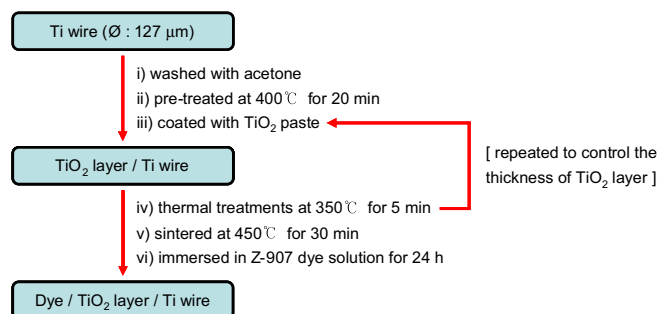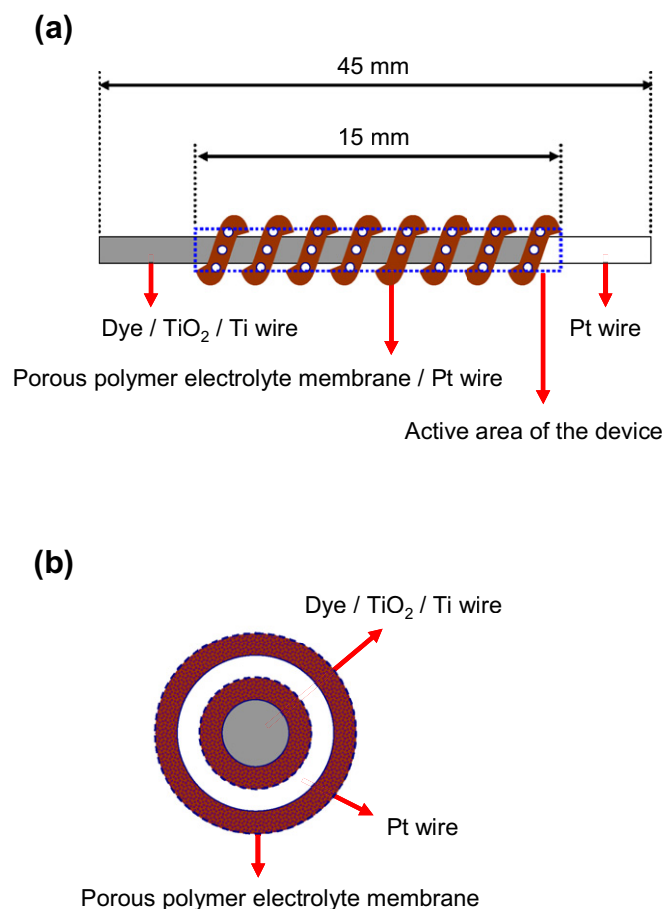

Fig. 2. Schematic illustration of the quasi-solid-state dye-sensitized photovoltaic fiber; (a) Longitudinal view and (b) cross-sectional view.

provide high ionic conductivity and good mechanical strength to the photovoltaic fiber. A dye-adsorbed TiO_2 coated titanium (Ti) wire is used as the working electrode and a platinum (Pt) wire is used as the counter electrode. Porous polymer membranes are prepared by the phase inversion method and immersed in a liquid-state electrolyte, producing the porous polymer electrolyte membrane that is applied to the counter electrode. The effect of pore size, pore volume and pore size distribution of the porous polymer electrolyte membranes on the photovoltaic characteristics of the quasi-solid-state dye-sensitized photovoltaic fibers is considered and the optimum thickness of the TiO_2 layer is
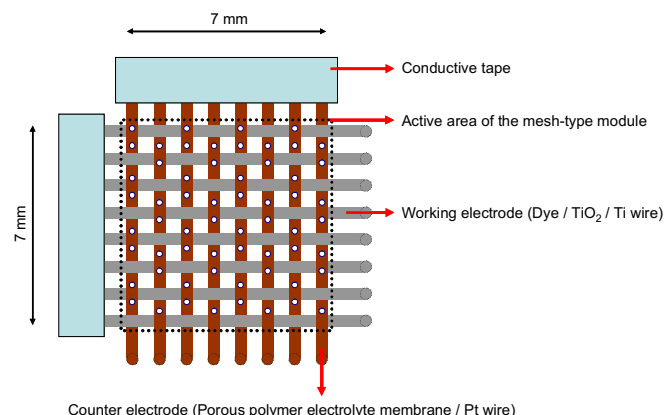

Fig. 1. Flow chart for the preparation of working electrodes.

Fig. 3. Schematic illustration of the mesh-type module having a plain weave structure.

determined. The twist pitch length of the counter electrode is also optimized. Finally, the possibility for large-scale application is investigated by fabricating a plain weave mesh-type module.

2. Experimental

2.1. Preparation of the working electrode

A Ti wire (Sigma–Aldrich) with a diameter of 127 μm was used as the photoelectrode substrate. The Ti wire was thoroughly washed with acetone using sonication and was pre-treated at 400 °C for 20 min to improve the adhesion of TiO_2 paste and to increase the electron transport efficiency. Upon heat treatment, the color of the Ti wire changed from gray to dark-blue. The pre-treated Ti wire was uniformly coated with a commercial TiO_2 paste (15–20 nm anatase particles, D-L series, Solaronix) using a nano dip coater (MD-0408-S2, SDI Co., Ltd.) and subsequently subjected to a 5 min thermal treatment at 350 °C. The thickness of the TiO_2 layer was controlled by repeating the dip-coating process multiple times. The TiO_2 layer coated Ti wire was then sintered in a furnace
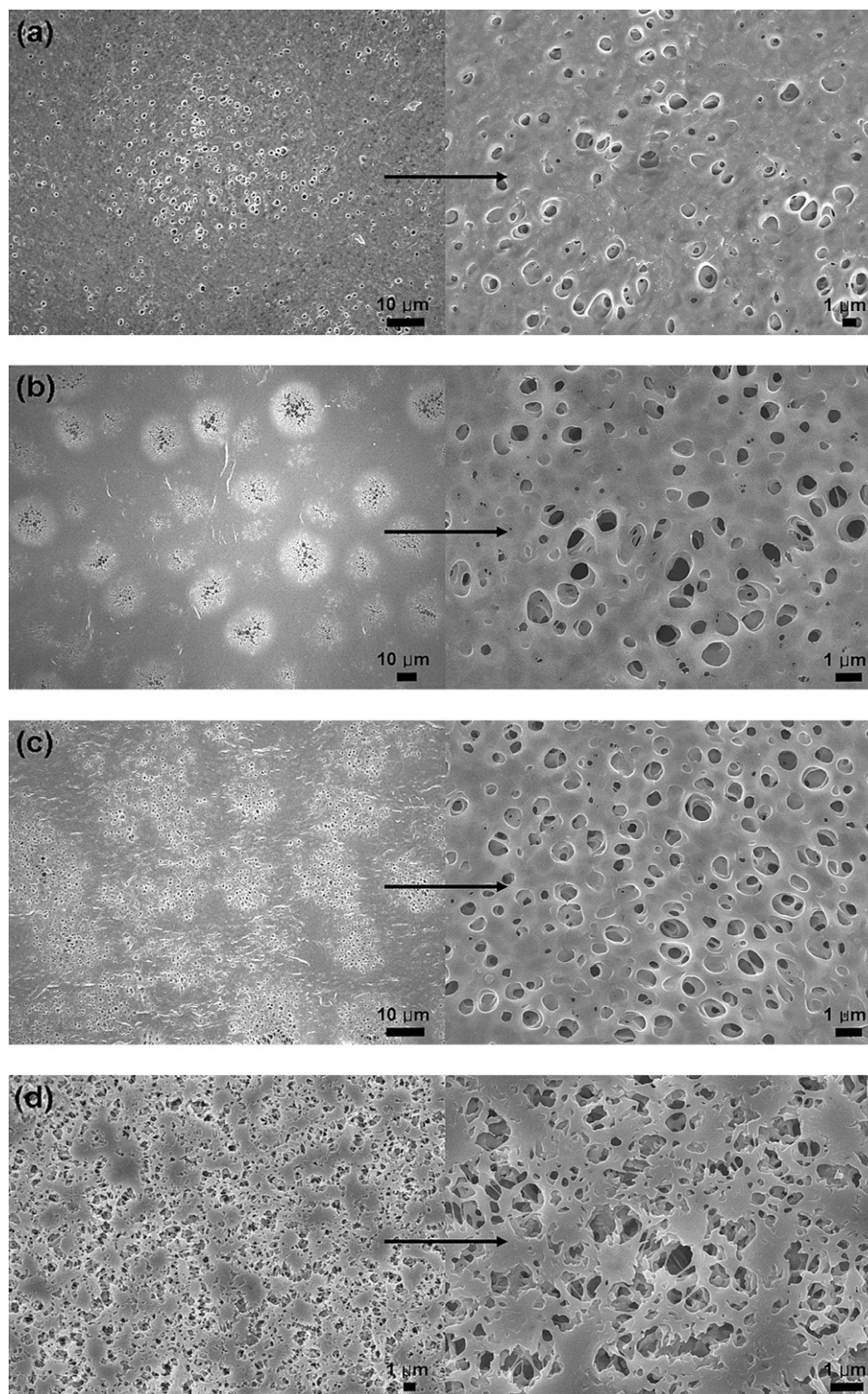

Fig. 4. Surface morphology of the PVdF-HFP/P123 porous polymer membranes with various P123 content; (a) 0 wt.%, (b) 25 wt.%, (c) 50 wt.% and (d) 75 wt.%.

(WiseTherm, Daihan Scientific) at 450 °C for 30 min, slowly cooled to 25 °C, and subsequently immersed in an ethanol solution containing 0.5 mM of cis-bis(isothiocyanato) (2,2′-bipyridyl-4,4′-dicarboxylato) (2,2′-bipyridyl-4,4′-di-nonyl) ruthenium (II) (Z-907 dye, Dyesol) at room temperature for 24 h. Finally, the dye-adsorbed TiO₂ layer coated Ti wire was rinsed with ethanol and air-dried. The process for preparing the working electrode is illustrated in Fig. 1.

2.2. Preparation of the counter electrode coated with PVdF-HFP/P123 porous polymer electrolyte membranes

The counter electrode used in this study was a Pt wire (Sigma–Aldrich) with a diameter of 127 μm and the porous polymer electrolyte membranes were prepared by the phase inversion method introduced in the literature [37,39,40]. After a certain amount of PVdF-HFP (Kynar® 2801, Arkema) was dissolved in 1-methyl-2-pyrrolidinone (NMP, Sigma–Aldrich), polyethylene oxide-co-polypropylene oxide-co-polyethylene oxide (P123, D-BASF) was added to the PVdF-HFP solution. The PVdF-HFP copolymer was used as the matrix for polymer electrolyte where P123 was added to control the pore structure of the polymer membrane. Membranes with different pore structure were prepared by varying the P123 content (0, 25, 50 and 75 wt.%) in the PVdF-HFP/P123 blend polymer. After the P123 was completely dissolved under intensive stirring at 70 °C for 12 h, the PVdF-HFP/P123 solution was coated on the Pt wire using a dip coating process. Water was used as the nonsolvent to induce phase inversion, thus the PVdF-HFP/P123 solution coated Pt wire was immediately immersed in a water bath for about 1 h and then dried in a vacuum oven at 80 °C for 24 h. Finally, the PVdF-HFP/P123 porous polymer membrane coated Pt wire was immersed in an organic liquid-state electrolyte composed of 0.5 M LiI (Aldrich), 0.05 M I₂ (Samchun chemical), and 0.5 M 4-tertbutylpyridine (TBP, Aldrich) in acetonitrile (Junsei chemical) for 2 h to activate the porous polymer electrolyte membrane. To prepare samples for characterization of the porous polymer electrolyte membranes, a slide glass was coated with the PVdF-HFP/P123 solution using a doctor-blade method. The casting thickness of the PVdF-HFP/P123 solution was controlled to be identical to that of the PVdF-HFP/P123 coating on the Pt wire.

2.3. Assembly of the photovoltaic fiber and fabrication of the mesh-type module

The PVdF-HFP/P123 porous polymer electrolyte membrane coated Pt wire was twisted around the dye-adsorbed TiO₂ layer coated Ti wire to form a spiral and the assembled device was immersed in a liquid electrolyte once again. The projected area of the quasi-solid-state dye-sensitized photovoltaic fiber was determined by multiplying the diameter of photoelectrode and the length of device. A schematic illustration of the device is given in Fig. 2.

A mesh-type module was fabricated by hand weaving the electrodes in a plain-weave structure, with the working electrode as the weft and the counter electrode coated with the porous polymer electrolyte membrane as the warp. A total of 16 metal wires (8 per electrode) were used in the module, creating 49 meshes where the distance between each electrode was about 1 mm. The active area of the module was 0.49 cm² (0.7 cm × 0.7 cm). An aluminum foil conductive tape (DSS-507, DAESANG S.T. Co., Ltd.) was attached to the edge of the module in order to effectively collect current and to connect the module to an external circuit. A schematic illustration of the mesh-type module is presented in Fig. 3.
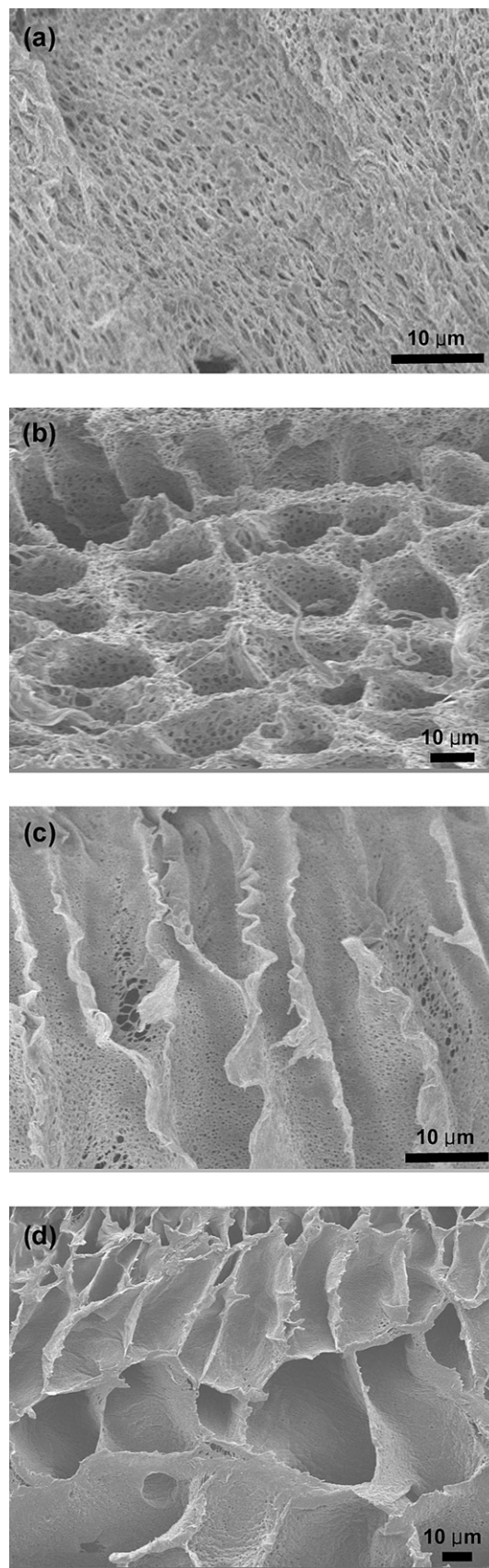

Fig. 5. Cross-sectional view of the PVdF-HFP/P123 porous polymer membranes with various P123 content; (a) 0 wt.%, (b) 25 wt.%, (c) 50 wt.% and (d) 75 wt.%.

Fig. 7. Electrolyte uptake and leakage of the PVdF-HFP/P123 porous polymer membranes with various P123 content.

a field-emission scanning electron microscope (FE-SEM, Supra 55VP, Carl Zeiss) and the pore size and pore size distribution of the polymer membranes were measured using an automatic porosimeter (Autopore IV 9500, Micromeritics).
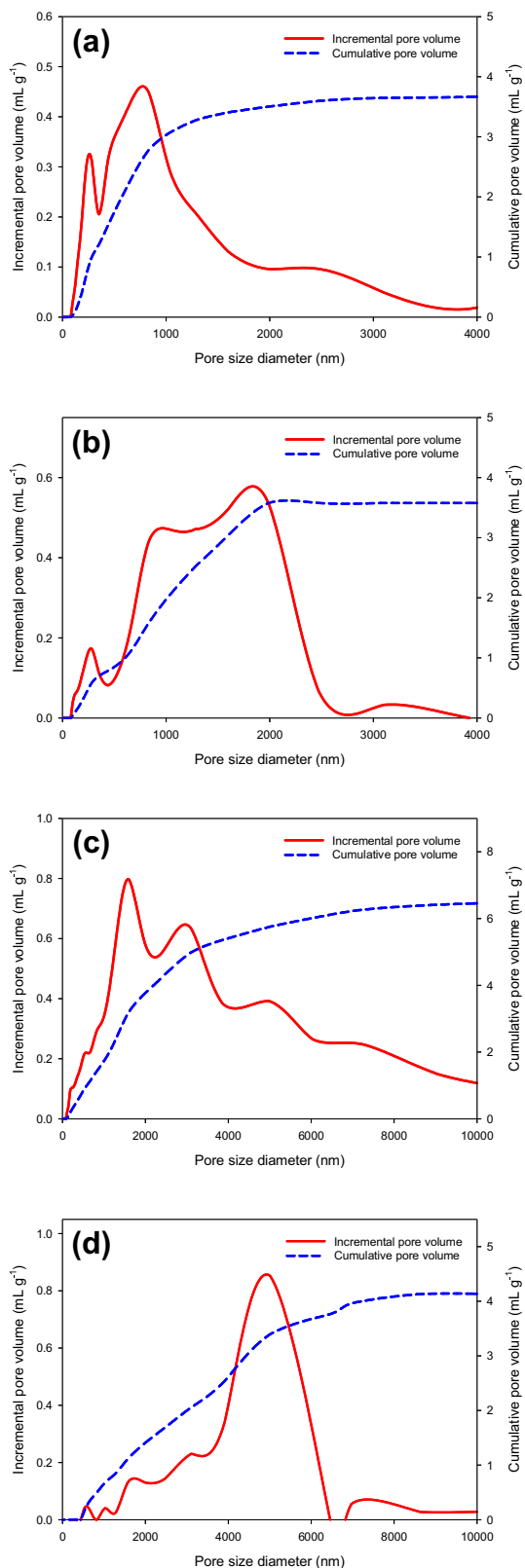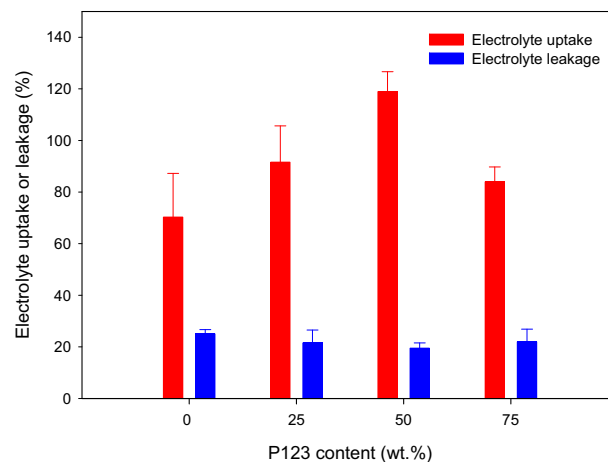

Fig. 6. Pore size distribution of the PVdF-HFP/P123 porous polymer membranes with various P123 content; (a) 0 wt.%, (b) 25 wt.%, (c) 50 wt.% and (d) 75 wt.%.

2.4. Characterization

The surface morphology of the PVdF-HFP/P123 porous polymer membranes and the thickness of TiO$_2$ layer was observed using
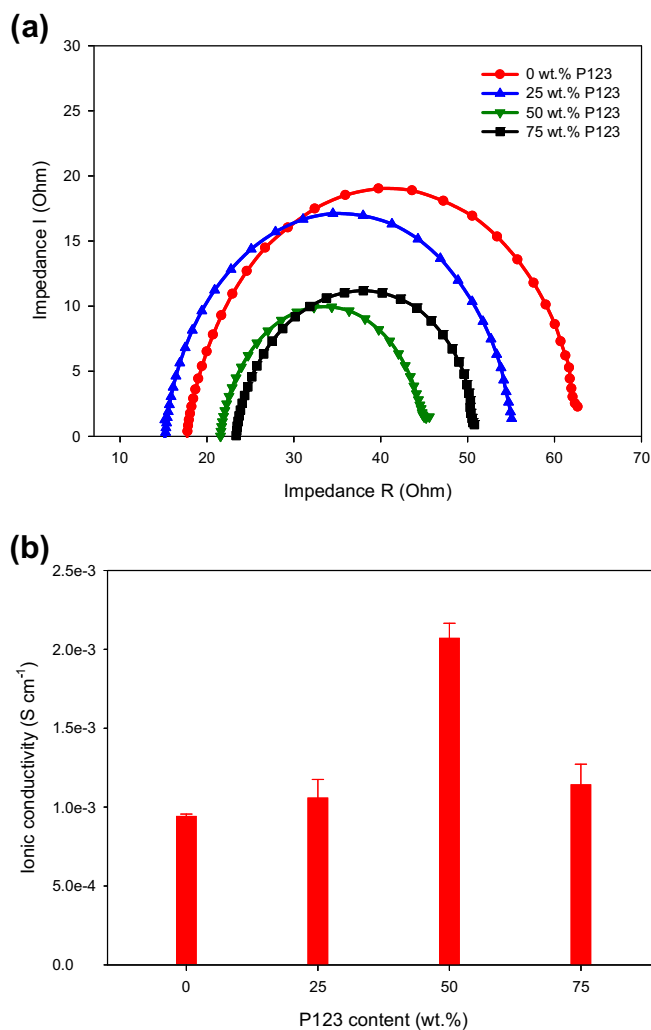
Fig. 8. (a) Nyquist plots and (b) ionic conductivity of the PVdF-HFP/P123 porous polymer electrolyte membranes with various P123 content.

In order to determine the electrolyte uptake and leakage of PVdF-HFP/P123 polymer membranes, a small piece of membrane (10 mm × 10 mm) was immersed in an electrolyte solution for about 2 h and was weighed every 10 min until no weight change occurred. The electrolyte uptake and leakage was determined by Eqs. (1) and (2).

$$\text{Electrolyte uptake} = (W_e - W_i)/W_i \tag{1}$$

$$\text{Electrolyte leakage} = (W_a - W_e)/(W_a - W_i) \tag{2}$$

where, W_i is the weight of porous polymer membrane, W_a and W_e are the initial weight and equilibrium weight of the membrane after immersion in electrolyte solution, respectively.

The ionic conductivity measurement of the PVdF-HFP/P123 porous polymer electrolyte membranes was preformed with an electrochemical impedance spectroscopy (EIS) system (IM6ex PP240, Zahner) in the 10 Hz ∼ 3 MHz frequency range at room temperature by sandwiching the polymer electrolyte membrane between two blocking Pt electrodes. The ionic conductivity (σ) was calculated by Eq. (3).

$$\sigma = t/AR_b \tag{3}$$

where, t is the thickness of the electrolyte membrane, A is the area of the electrolyte membrane, and R_b is the bulk resistance determined from the impedance plot.

The photocurrent−voltage (I−V) characteristics of the quasi-solid-state dye-sensitized photovoltaic fibers and the mesh-type module were measured under 100 mW cm^{-2} (AM 1.5) light intensity with a solar cell QE measurement system (K3000(IV), McScience) equipped with a xenon (Xe) short arc lamp.

3. Results and discussion

3.1. Surface morphology and pore size distribution of PVdF-HFP/P123 porous polymer membranes

The surface morphology of the porous polymer membranes with different blend ratios of P123 to PVdF-HFP is given in Fig. 4. Numerous pores are generated in the PVdF-HFP/P123 polymer membrane due to solvent exchange by diffusion between the solvent (NMP) and nonsolvent (water) during the phase inversion process, and no phase separation between PVdF-HFP and P123 is observed. As the P123 content increases, the number of pores in the polymer membrane increases, decreasing the membrane compactness. With 0 wt.% P123 (Fig. 4(a)), pores in the range of around 1−2 μm are locally distributed in the membrane, but as the P123 content increases, slightly larger pores are widely distributed throughout the membrane. Meanwhile, poor mechanical strength of the porous polymer membrane is observed at 75 wt.% P123 content.
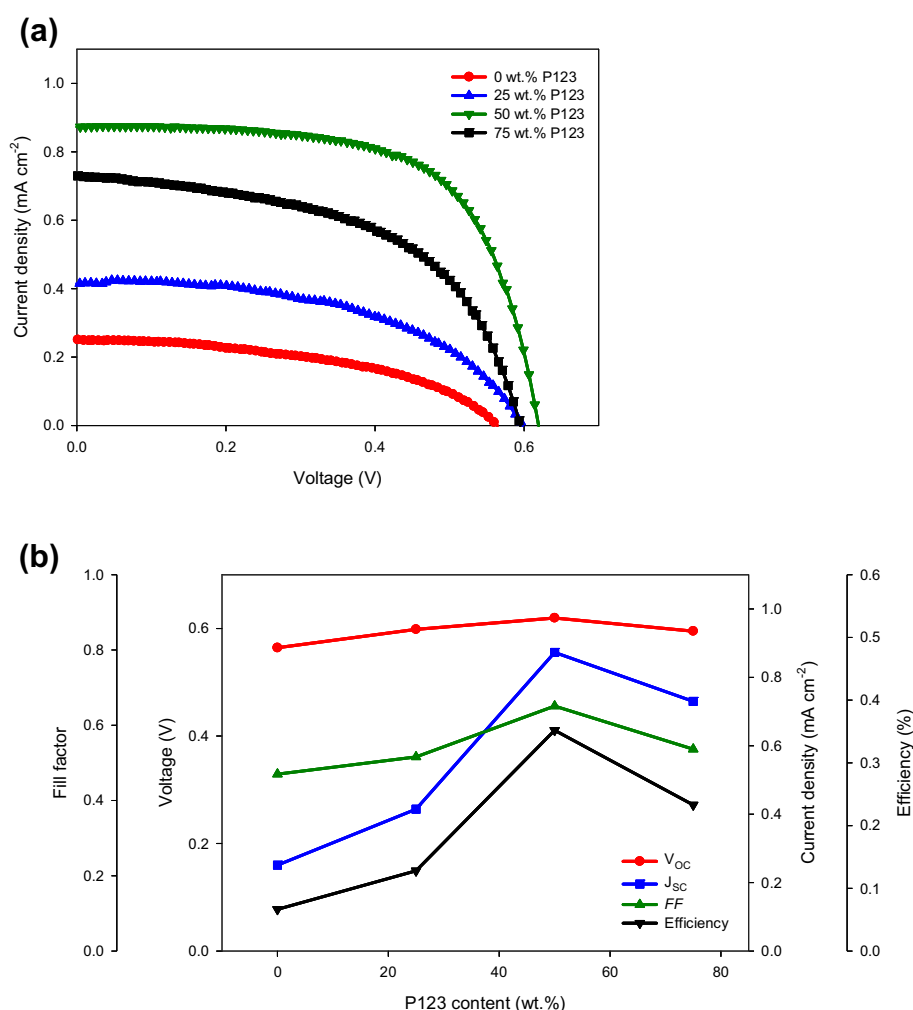

Fig. 9. Photocurrent−voltage characteristics of the quasi-solid-state dye-sensitized photovoltaic fibers with various P123 content; (a) I−V curves and (b) V_{oc}, J_{sc}, FF and η values.

Table 1
I–V parameters of the quasi-solid-state dye-sensitized photovoltaic fibers with various P123 content.

P123 blend ratio (wt.%)	J_{sc} (mA cm^{-2})	V_{oc} (V)	FF	η (%)
0	0.2509	0.5642	0.4701	0.06655
25	0.4147	0.5983	0.5158	0.1280
50	0.8730	0.6195	0.6510	0.3521
75	0.7298	0.5951	0.5363	0.2329

In the cross-sectional images shown in Fig. 5, the transformation of a sponge-like structure (Fig. 5(a)) to a honeycomb structure (Fig. 5(b)) as the P123 content increases is observed. When the P123 content reaches 50 wt.% and 75 wt.%, finger-like pathways in the through thickness direction of the polymer membrane is formed.

The thickness of all PVdF-HFP/P123 porous polymer membrane is about 80 μm.

The pore size distributions of the PVdF-HFP/P123 porous polymer membranes are given in Fig. 6. As observed in Fig. 4, the pore size distribution gradually broadens and the pore volume increases as the P123 content in the membrane increases. With 0 wt.% and 25 wt.% P123, a relatively narrow distribution pattern is observed around pore sizes 1–2 μm. But with P123 content of 50 wt.% and 75 wt.%, the range of pore size expands up to 6–10 μm and the pore size distribution broadens. The cumulative pore volume also increases due to the increase in both the number and size of pores. The cumulative pore volume of the membrane with 75 wt.% P123, however, is significantly lower than that of the membrane with 50 wt.% P123. Judging from the changes in surface morphology and
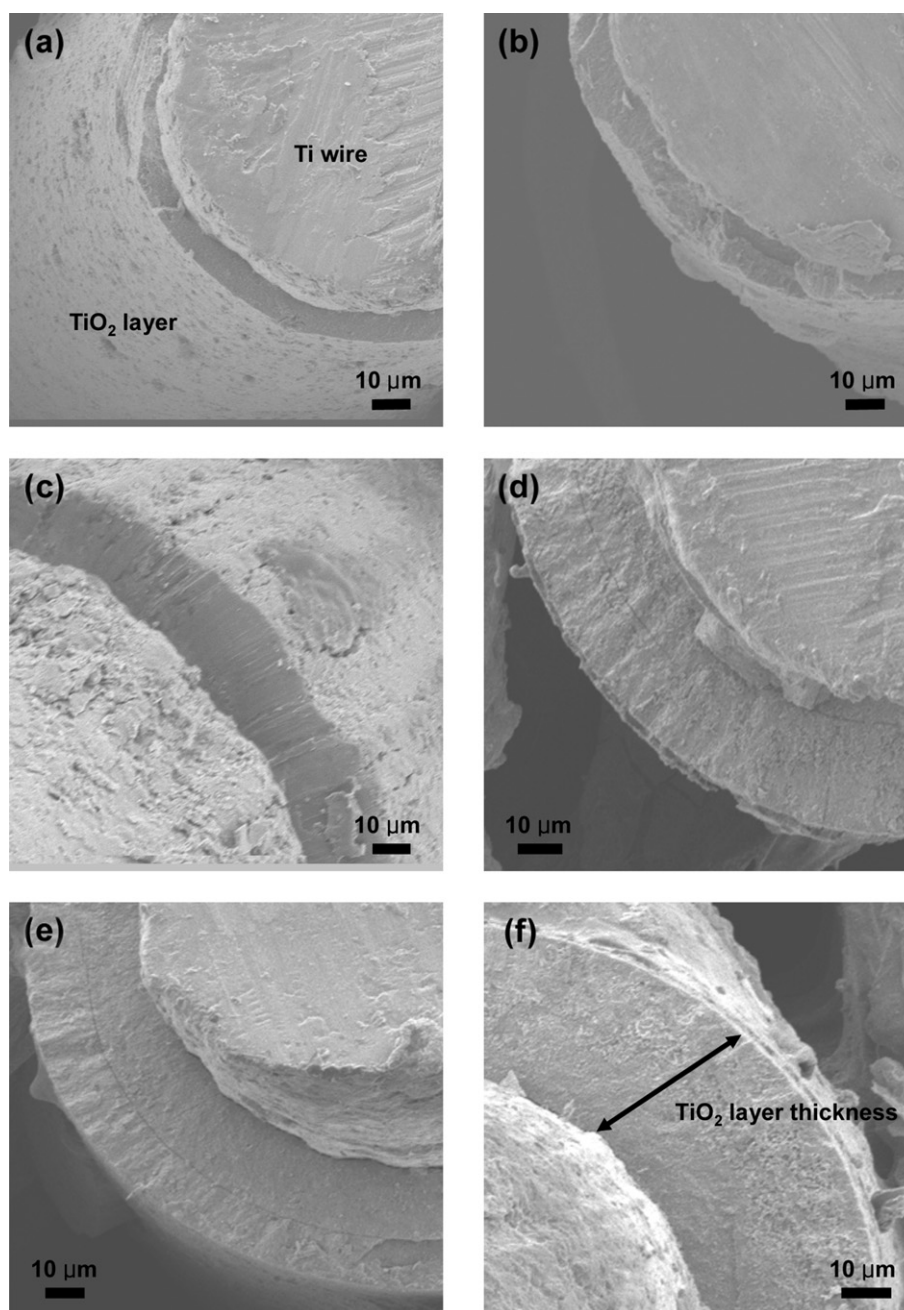

Fig. 10. FE-SEM images of the Ti wires coated with various thicknesses of TiO$_2$ layer; (a) dip-coated 5 times (8.1 μm), (b) dip-coated 11 times (11.2 μm), (c) dip-coated 35 times (23.4 μm), (d) dip-coated 47 times (29.7 μm), (e) dip-coated 55 times (32.9 μm), and (f) dip-coated 63 times (36.5 μm).

pore size distribution of the PVdF-HFP/P123 polymer membrane caused by the addition of P123 to PVdF-HFP, the effect of P123 can be attributed to two factors; (i) Due to the higher solubility of P123 in NMP, PVdF-HFP/P123 is more homogeneously dispersed in NMP than 100% PVdF-HFP, resulting in a more dense pore structure upon phase inversion. (ii) Because P123 is a water-soluble polymer, extraction of P123 chains by water during the phase inversion process formed membranes with higher pore volume. Such enhanced pore properties by the addition of P123 is expected to increase the liquid electrolyte uptake and enhance the contact between the electrolyte and electrode.

3.2. Electrolyte uptake, leakage and ionic conductivity of the PVdF-HFP/P123 porous polymer membranes

The electrolyte uptake and leakage of the PVdF-HFP/P123 porous polymer membranes with various P123 content is shown in Fig. 7. The weight change in the polymer membranes was measured every 10 min after absorbing excess electrolyte solution from the membrane surface using a filter paper. As can be seen in the figure, electrolyte uptake of the porous polymer membranes increases with higher P123 content. Efficient encapsulation of the electrolyte is possible by the increased pore volume of membranes with higher P123 content, and the affinity between P123 and the electrolyte solution also plays a role in increasing the uptake. When the P123 content reaches 75 wt.%, however, the electrolyte uptake decreases due to the decrease in cumulative pore volume, despite the increased pore size (Fig. 6(d)). In contrast to the electrolyte uptake, the electrolyte leakage of the porous polymer membranes decreases as the P123 content increases up to 50 wt.%. The membrane with 50 wt.% P123 shows the maximum electrolyte uptake of 119% and the minimum electrolyte leakage of 19%.

The Nyquist plots and ionic conductivity of the PVdF-HFP/P123 porous polymer electrolyte membrane with various amounts of P123 is given in Fig. 8. The ionic conductivity obtained using the real x-axis intercept of the Nyquist plots increases with increasing P123 content up to 50 wt.%. This is due to the increased electrolyte uptake by the larger pore size and pore volume. Especially, the ionic conductivity of the membrane with 50 wt.% P123 shows a large increase from that of the membrane with 25 wt.% P123, giving a value of 2.07×10^{-3} S cm^{-1}. The large jump in ionic conductivity is attributed to the finger-like pathways formed in the through-thickness direction of the membrane as well as the increase in electrolyte uptake. The finger-like pathways allow free flow of the electrolyte solution within the membrane which is difficult in sponge-like (0 wt.% P123) or honeycomb (25 wt.% P123) pore structures. These results are consistent with the results of surface morphology and pore size distribution shown in Figs. 4–6.

3.3. Photovoltaic performances of the quasi-solid-state dye-sensitized photovoltaic fibers

3.3.1. Effect of P123 content

The I–V characteristics of quasi-solid-state dye-sensitized photovoltaic fibers with varying P123 content are given in Fig. 9 and their photovoltaic parameters are summarized in Table 1. In all cases, the thickness of the TiO$_2$ layer and PVdF-HFP/P123 porous polymer electrolyte membrane is controlled to 11.2 μm and 80 μm, respectively, and the twist pitch length of the counter electrode is set to about 1 mm. The short-circuit current density (J_{sc}) improves as the P123 content increases, reaching a maximum of 0.8730 mA cm^{-2} at 50 wt.% P123. The increased pore volume and electrolyte uptake of the polymer membranes with higher P123 content enhances the contact property between the electrode and electrolyte, and increases the ionic conductivity of polymer
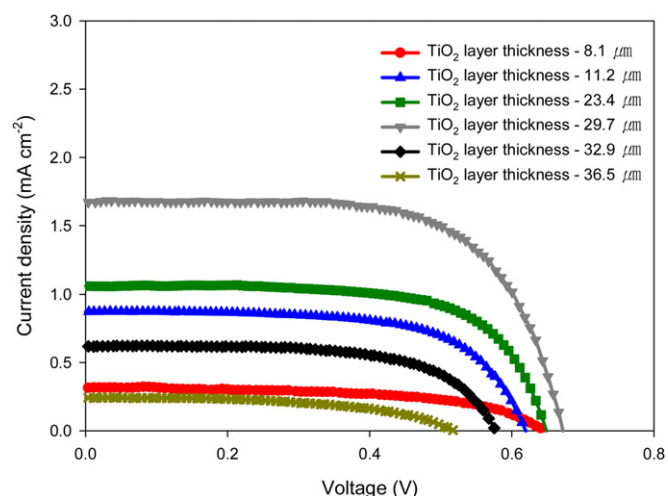

Fig. 11. I–V curves of the quasi-solid-state dye-sensitized photovoltaic fibers with different thicknesses of TiO$_2$ layer.

electrolyte membrane. Such enhanced ionic conductivity decreases the overall inner resistance of the photovoltaic fibers leading to an improved J_{sc}. When the P123 content reaches 75 wt.%, however, the J_{sc} slightly decreases due to the reduced ionic conductivity of the electrolyte membrane. The open-circuit voltage (V_{oc}), which value is determined by the energy level difference between the Fermi level of the TiO$_2$ photoelectrode and the redox potential of the I^-/I_3^- electrolyte, is maintained almost unchanged regardless of the P123 content. The fill factor (FF), which is affected by the series and shunt resistances of the whole device, increases with higher P123 content but decreases at 75 wt.% P123. The increased FF is due to the reduced internal resistance in the photovoltaic fibers by the enhanced ionic conductivity. The quasi-solid-state dye-sensitized photovoltaic fiber containing a PVdF-HFP/P123 porous polymer electrolyte membrane with 50 wt.% P123 performs the best, exhibiting a J_{sc} of 0.8730 mA cm^{-2}, a V_{oc} of 0.6195 V, and a FF of 0.6510. Whereas the photovoltaic fiber containing a membrane with 75 wt.% P123 is exposed to device stability problems due to its poor mechanical strength.

3.3.2. Effect of TiO$_2$ layer thickness

The FE-SEM images in Fig. 10 show the TiO$_2$ layers of different thicknesses on Ti wires. The TiO$_2$ layer is firmly attached to the Ti wire without any observed gaps. The measured thickness of the TiO$_2$ layer is in the range of 8.1–36.5 μm, depending on how many times the Ti wire was subjected to dip coating. More specifically, the thickness of the TiO$_2$ layers are about 8.1 μm (5 times), 11.2 μm (11 times), 23.4 μm (35 times), 29.7 μm (47 times), 32.9 μm (55 times), and 36.5 μm (63 times).

The I–V curves of the quasi-solid-state dye-sensitized photovoltaic fibers that were fabricated with Ti wires coated with different thicknesses of TiO$_2$ layer are shown in Fig. 11 and their photovoltaic parameters are summarized in Table 2. The

Table 2
I–V parameters of the quasi-solid-state dye-sensitized photovoltaic fibers with different thicknesses of TiO$_2$ layer.

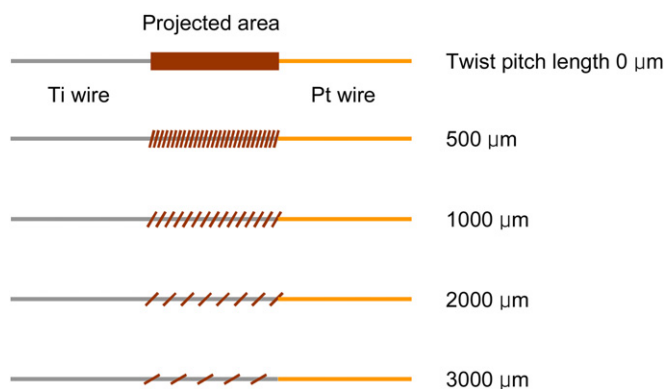| TiO$_2$ layer thickness (μm)	J_{sc} (mA cm^{-2})	V_{oc} (V)	FF	η (%)
8.1	0.3139	0.6449	0.5676	0.1149
11.2	0.8730	0.6195	0.6510	0.3521
23.4	1.061	0.6488	0.6691	0.4606
29.7	1.671	0.6719	0.6675	0.7494
32.9	0.6191	0.5778	0.6391	0.2286
36.5	0.2420	0.5190	0.5270	0.06619

Fig. 12. Schematic illustration of the quasi-solid-state dye sensitized photovoltaic fibers with counter electrodes having different twist pitch lengths.

Table 3
$I–V$ parameters of the quasi-solid-state dye-sensitized photovoltaic fibers with varying twist pitch lengths of counter electrode.

Counter electrode twist pitch length (μm)	J_{sc} (mA cm^{-2})	V_{oc} (V)	FF	η (%)
500	2.117	0.6932	0.7015	1.029
1000	1.671	0.6675	0.7494	
2000	0.6317	0.5770	0.5358	0.1953
3000	0.5437	0.4702	0.5108	0.1306

photovoltaic fibers were prepared with counter electrodes coated with 50 wt.% P123 membranes, which exhibited the maximum photovoltaic performance in the previous section. The J_{sc} increases as the thickness of the TiO$_2$ layer increases. As J_{sc} is related to the electron injection rate into the conduction band of TiO$_2$ from the photo-excited dye, the increase in the amount of dye adsorbed on the thicker TiO$_2$ layers increases the number of photogenerated electrons, which eventually increases the J_{sc}. When the TiO$_2$ layer thickness reaches 32.9 μm and over, however, the J_{sc} decreases significantly. This is due to the increase in charge recombination between the electron injected into the conduction band of TiO$_2$ and the redox electrolyte. On the other hand, the V_{oc} decreases from 0.6449 V to 0.5190 V as the thickness of the TiO$_2$ layer increases due to the increase in charge recombination or back electron transfer. The FF also decreases as the series resistance of the device increases. The quasi-solid-state dye-sensitized photovoltaic fiber having a 29.7 μm-thick TiO$_2$ layer performs the best, exhibiting a J_{sc} of 1.671 mA cm^{-2}, a V_{oc} of 0.6719 V and a FF of 0.6675.

3.3.3. Effect of counter electrode twist pitch length

The pitch length of the twisted counter electrode is another crucial factor that affects the characteristics of quasi-solid-state dye-sensitized photovoltaic fibers. To investigate the effect of twist pitch length of the counter electrode, quasi-solid-state dye-sensitized photovoltaic fibers were prepared with four different pitch lengths (500, 1000, 2000 and 3000 μm). A schematic illustration of the photovoltaic fibers with various twist pitch lengths is

given in Fig. 12. A device with twist pitch length of 0 μm was not prepared because the amount of sunlight reaching the working electrode would be too limited if the counter electrode fully wrapped the working electrode.

The effect of twist pitch length of the counter electrode on the photovoltaic performances of the quasi-solid-state dye-sensitized photovoltaic fibers is shown in Fig. 13. A 50 wt.% P123 porous polymer membrane was used and the working electrode was coated with a 29.7 μm-thick TiO$_2$ layer. As can be seen from Fig. 13, all photovoltaic parameters (i.e. J_{sc}, V_{oc}, and FF) decreases significantly as the twist pitch length of counter electrode increases. Lengthening the twist pitch reduces the contact area between the working electrode and the counter electrode, and increases the electron transport distance inside the photovoltaic fibers. Such changes obstruct the regeneration of oxidized dyes, increase the charge trapping or recombination in surface state and increase the internal resistance of the devices. As a result, the J_{sc}, V_{oc}, and FF decreases with increasing twist pitch length. The maximum performance of the quasi-solid-state dye-sensitized photovoltaic fiber is obtained with 500 μm twist pitch length, yielding an energy conversion efficiency (η) of 1.029%. The photovoltaic parameters of the photovoltaic fibers with different twist pitch lengths are summarized in Table 3.

3.4. Photovoltaic performances of a mesh-type module

The feasibility for large-scale commercial application is an essential factor to be considered when developing photovoltaic fibers. In this study, a mesh-type module composed of dye-adsorbed TiO$_2$ layer coated Ti wires and PVdF-HFP/P123 porous polymer electrolyte membrane coated Pt wires was fabricated in a plain weave structure. The TiO$_2$ layer was 29.7 μm-thick and a 50 wt.% P123 porous membrane was used. The $I–V$ curve of the mesh-type module fabricated in this study is given in Fig. 14. The
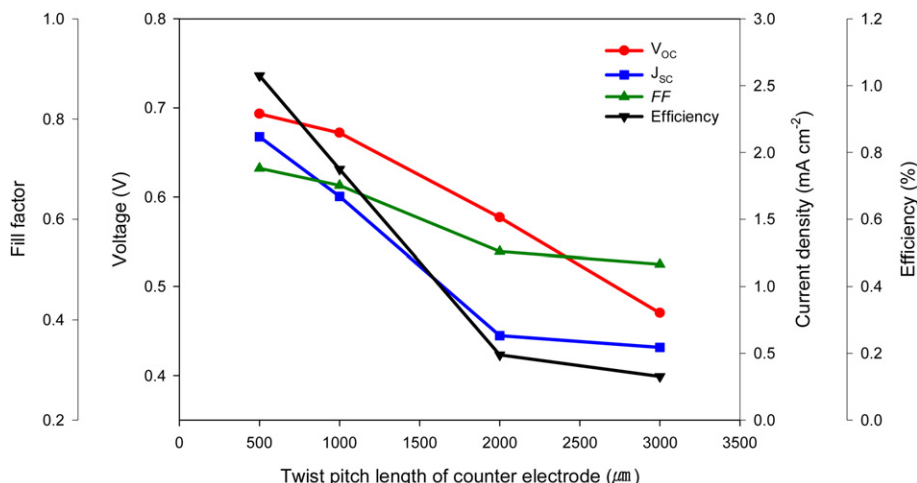

Fig. 13. Photovoltaic characteristics of the quasi-solid-state dye sensitized photovoltaic fibers with counter electrodes having different twist pitch lengths.
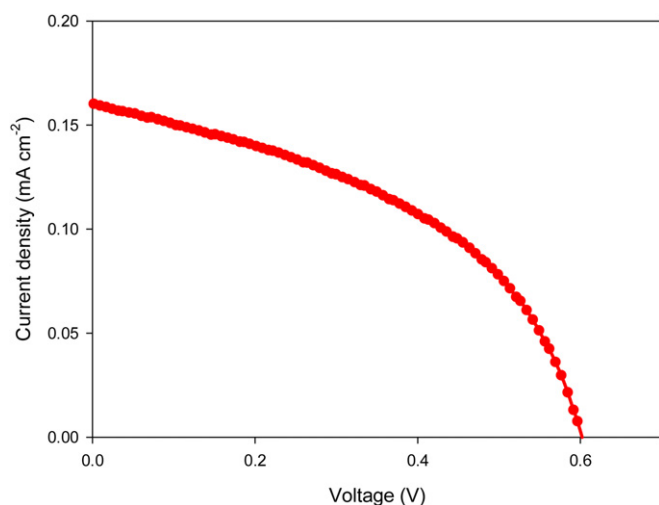
Fig. 14. *I–V* curve of the mesh-type module based on a plain weave structure.

module showed photovoltaic characteristics with promising potential: $J_{sc} = 0.1601$ mA cm^{-2}, $V_{oc} = 0.6021$ V, $FF = 0.4485$ and $\eta = 0.04323\%$. A few causes for the generally low performance of the module are: the loose structure of the module, which reduces the active area (*i.e.* there are relatively large empty spaces between electrodes within the active area); defects formed in the TiO$_2$ layer during the device assembly process; as well as the contact resistance between the electrodes and the conductive tape, which was used to connect the module to an external circuit. Thus, further work is required for the fabrication of efficient mesh-type modules with high conversion efficiency.

4. Conclusions

Quasi-solid-state dye-sensitized photovoltaic fibers containing PVdF-HFP/P123 porous polymer electrolyte membranes are fabricated and their photovoltaic performances are investigated. A dye-adsorbed TiO$_2$ layer coated Ti wire and Pt wire is used as the working electrode and counter electrode, respectively. The TiO$_2$ layer is firmly attached to the Ti wire by the dipping process and its thickness is controlled by the number of times that the Ti wire is subjected to dip-coating. The PVdF-HFP/P123 porous polymer membranes prepared by the phase inversion technique are applied to the counter electrode and are immersed in a liquid-state electrolyte for 2 h to activate the porous polymer electrolyte membranes. The pore size and pore size distribution of the PVdF-HFP/P123 polymer membranes are adjusted by varying the P123 content. The pore volume of the polymer membrane increases with increased P123 content, facilitating the electrolyte uptake, which improves the ionic conductivity of porous polymer electrolyte membrane. The photovoltaic characteristics of the quasi-solid-state dye-sensitized photovoltaic fibers increase with increased P123 content due to the enhanced ionic conductivity of electrolyte membrane. Also, the photovoltaic performances of the photovoltaic fibers are found to be significantly dependent upon the TiO$_2$ layer thickness and the twist pitch length of the counter electrode. The quasi-solid-state dye-sensitized photovoltaic fiber providing maximum performance is that with a 50 wt.% P123 membrane, 29.7 μm-thick TiO$_2$ layer and 500 μm twist pitch length, and exhibits a performance of $J_{sc} = 2.117$ mA cm^{-2}, $V_{oc} = 0.6932$ V, $FF = 0.7015$, and $\eta = 1.029\%$. The feasibility of large-scale application of the quasi-solid-state dye-sensitized photovoltaic fibers is confirmed by a mesh-type module based on the fiber-like electrodes. Although the conversion efficiency of the quasi-solid-state dye-sensitized photovoltaic fibers proposed in this study is relatively low compared to planar DSSCs based on solid-state electrolytes, the photovoltaic performances are expected to be enhanced by altering the thickness of the porous polymer electrolyte membrane and the diameter of metal wire electrodes, etc. Future work will include the development of highly efficient all solid-state dye-sensitized photovoltaic fibers with long-term durability as well as the fabrication of large-scale modules for the practical applications of DSSCs.

Acknowledgment

References

[1] B. O'Regan, M. Gratzel, Nature 353 (1991) 737–740.
[2] C.S. Chou, M.G. Guo, K.H. Liu, Y.S. Chen, Appl. Energy 92 (2012) 224–233.
[3] F.T. Kong, S.Y. Dai, K.J. Wang, Adv. OptoElectron. 2007 (2007) 1–13.
[4] Y. Liu, H. Wang, H. Shen, W. Chen, Appl. Energy 87 (2010) 436–441.
[5] D. Zou, D. Wang, Z. Chu, Z. Lv, X. Fan, Coord. Chem. Rev. 254 (2010) 1169–1178.
[6] M. Toivola, J. Halme, K. Miettunen, K. Aitola, P.D. Lund, Int. J. Energy Res. 33 (2009) 1145–1160.
[7] M.G. Kang, N.G. Park, K.S. Ryu, S.H. Chang, K.J. Kim, Sol. Energy Mater. Sol. Cells 90 (2006) 574–581.
[8] M. Durr, A. Schmid, M. Obermaier, S. Rosselli, A. Yasuda, G. Nelles, Nat. Mater. 4 (2005) 607–611.
[9] K. Miettunen, J. Halme, P. Vahermaa, T. Saukkonen, M. Toivola, P. Lund, J. Electrochem. Soc. 156 (2009) B876–B883.
[10] J.J. Kim, K.S. Kim, G.Y. Jung, J. Mater. Chem. 21 (2011) 7730–7735.
[11] C.Y. Jiang, X.W. Sun, K.W. Tan, G.Q. Lo, A.K.K. Kyaw, D.L. Kwong, Appl. Phys. Lett. 92 (2008) 143101.
[12] A.F. Nogueira, C. Longo, M.-A. De Paoli, Coord. Chem. Rev. 248 (2004) 1455–1468.
[13] T. Yamaguchi, N. Tobe, D. Matsumoto, H. Arakawa, Chem. Commun. 45 (2007) 4767–4769.
[14] K.M. Lee, Y.C. Hsu, M. Ikegami, T. Miyasaka, K.R.J. Thomas, J.T. Lin, K.C. Ho, J. Power Sources 196 (2011) 2416–2421.
[15] H.C. Weerasinghe, P.M. Sirimanne, G.P. Simon, Y.B. Cheng, J. Photochem. Photobiol. A Chem. 206 (2009) 64–70.
[16] X. Fan, Z. Chu, F. Wang, C. Zhang, L. Chen, Y. Tang, D. Zou, Adv. Mater. 20 (2008) 592–595.
[17] J. Ramier, C.J.G. Plummer, Y. Leterrier, J.-A.E. Manson, B. Eckert, R. Gaudiana, Renew. Energy 33 (2008) 314–319.
[18] J. Ramier, N.D. Costa, C.J.G. Plummer, Y. Leterrier, J.-A.E. Manson, R. Eckert, R. Gaudiana, Thin Solid Films 516 (2008) 1913–1919.
[19] H. Wang, Y. Liu, M. Li, H. Huang, M. Zhong, H. Shen, Appl. Phys. A 97 (2009) 25–29.
[20] Q.-B. Meng, K. Takahashi, X.-T. Zhang, I. Sutanto, T.N. Rao, O. Sato, A. Fujishima, H. Watanabe, T. Nakamori, M. Uragami, Langmuir 19 (2003) 3572–3574.
[21] G.R.A. Kumara, A. Konno, K. Shiratsuchi, J. Tsukahara, K. Tennakone, Chem. Mater. 14 (2002) 954–955.
[22] L. Schmidt-Mende, M. Gratzel, Thin Solid Films 500 (2006) 296–301.
[23] H. Matsui, K. Okada, T. Kitamura, N. Tanabe, Sol. Energy Mater. Sol. Cells 93 (2009) 1110–1115.
[24] P. Wang, S.M. Zakeeruddin, J.-E. Moser, M. Gratzel, J. Phys. Chem. B 107 (2003) 13280–13285.
[25] R. Kawano, H. Matsui, C. Matsuyama, A. Sato, Md.A.B.H. Susan, N. Tanabe, M. Watanabe, J. Photochem. Photobiol. A Chem. 164 (2004) 87–92.
[26] J. Wu, Z. Lan, J. Lin, M. Huang, S. Hao, T. Sato, S. Yin, Adv. Mater. 19 (2007) 4006–4011.
[27] E. Stathatos, P. Lianos, A.S. Vuk, B. Orel, Adv. Funct. Mater. 14 (2004) 45–48.
[28] Y. Ren, Z. Zhang, S. Fang, M. Yang, S. Cai, Sol. Energy Mater. Sol. Cells 71 (2002) 253–259.
[29] R. Komiya, L. Han, R. Yamanaka, A. Islam, T. Mitate, J. Photochem. Photobiol. A Chem. 164 (2004) 123–127.
[30] G.P. Kalaignan, M.S. Kang, Y.S. Kang, Solid State Ion. 177 (2006) 1091–1097.
[31] M. Toivola, M. Ferenets, P. Lund, A. Harlin, Thin Solid Films 517 (2009) 2799–2802.
[32] X. Fan, Z. Chu, L. Chen, C. Zhang, F. Wang, Y. Tang, J. Sun, D. Zou, Appl. Phys. Lett. 92 (2008) 113510.
[33] D. Wang, S. Hou, H. Wu, C. Zhang, Z. Chu, D. Zou, J. Mater. Chem. 21 (2011) 6383–6388.

[34] J. Yu, D. Wang, Y. Huang, X. Fan, X. Tang, C. Gao, J. Li, D. Zou, K. Wu, Nanoscale Res. Lett. 6 (2011) 94–102.
[35] K.M. Kim, J.C. Kim, K.S. Ryu, Macromol. Mater. Eng. 291 (2006) 1495–1502.
[36] J. Cao, B. Zhu, D. Zuo, Y. Xu, J. Li, Chin. J. Polym. Sci. 26 (2008) 13–21.
[37] C.G. Wu, M.-I. Lu, H.J. Chuang, Polymer 46 (2005) 5929–5938.
[38] J.H. Kim, H.S. Jung, Y.S. Chi, T.J. Kang, Sol. Energy 86 (2012) 2606–2612.
[39] X. Zhang, C.-X. Wang, F.-Y. Li, Y.-Y. Xia, J. Photochem. Photobiol. A Chem. 194 (2008) 31–36.
[40] D.W. Kim, Y.B. Jeong, S.H. Kim, D.Y. Lee, J.S. Song, J. Power Sources 149 (2005) 112–116.